# Droplet-on-a-wristband: Chip-to-chip digital microfluidic interfaces between replaceable and flexible electrowetting modules†

**Shih-Kang Fan,*[ab] Hanping Yang[b] and Wensyang Hsu*[b]**

*Received 8th July 2010, Accepted 14th September 2010*
**DOI: 10.1039/c0lc00178c**



We present a long (204 mm), curved (curvature of 0.04 $mm^{-1}$), and closed droplet pathway in "droplet-on-a-wristband" (DOW) with the designed digital microfluidic modular interfaces for electric signal and droplet connections based on the study of electrowetting-on-dielectric (EWOD) in inclined and curved devices. Instead of using sealed and leakage-proof pipes to transmit liquid and pumping pressure, the demonstrated modular interface for electrowetting-driven digital microfluidics provides simply electric and fluidic connections between two adjacent parallel-plate modules which are easy-to-attach/detach, showing the advantages of using droplets for microfluidic connections between modules. With the previously reported digital-to-channel interfaces (Abdelgawad *et al.*, Lab Chip, 2009, **9**, 1046–1051), the chip-to-chip interface presented here would be further applied to continuous microfluidics. Droplet pumping across a single top plate gap and through a modular interface with two gaps between overlapping plates are investigated. To ensure the droplet transportation in the DOW, we actuate droplets against gravity in an inclined or curved device fabricated on flexible PET substrates prepared by a special razor blade cutter and low temperature processes. Pumping a 2.5 μl droplet at a speed above 105 mm $s^{-1}$ is achieved by sequentially switching the entire 136 driving electrodes (1.5 mm × 1.5 mm) along the four flexible modules of the DOW fabricated by 4-inch wafer facilities.

## Introduction

Incorporating functional microcomponents, such as heaters, mixers, filters, and sensors, into a microfluidic device to perform sophisticated chemical or biological tasks has been intensively studied,[1–5] showing the large scale integration[6–10] would be one of the approaches to lab-on-a-chip (LOC). Alternatively, complicated LOC composing replaceable microfluidic modules for individual tasks, including sample preconcentration, separation, and detection, would become important when monolithically integrated LOC is too costly and complex. However, few modular LOCs have been reported because the interface between modules is challenging.[11–14] For a fluid driven continuously by pressure in a microchannel within one of the modules, the modular interface needs to transmit not only the fluid but also the pumping pressure. As a result, robust and sealed tubing connecting microchannels and modules would be necessary, which causes large dead volume[11] and hinders the replacement of the modules. Hence special interfacing between chips using barbed connectors,[12] microfluidic breadboards,[13] miniaturized luer fittings,[14] and MEMS o-rings[15] would be necessary for modular LOC. The earlier reported microfluidic connector techniques[16,17] mainly focused on the world-to-chip interfaces, which are not suitable for compact LOC with numerous modules.

Compared with pressure-driven continuous flow in microchannels, pumping droplets by electrowetting, or electrowetting-on-dielectric (EWOD),[18,19] is more feasible for modular LOC. It is because the pumping pressure to drive a droplet would be locally generated by electrowetting at any two ends of a droplet even across a gap between two closely neighbored modules. Instead of preserving the pumping pressure across a well-aligned and leakage-proof interface for the continuous flow microfluidics, the modular interface for digital (droplet-based) microfluidics simply requires to provide proper electric connections for electrowetting actuations between easy-to-attach/detach modules. The digital microfluidic modular interfaces presented here can be further applied as a gateway technology to exchange fluids between two continuous flow microfluidic devices with proper digital-to-channel interfaces.[20] Although modules with analysis or detection functionalities are not shown here, we focus on the modular interface and demonstrate wearable (8-inch in circumference) "droplet-on-a-wristband" (DOW) composed of four flexible modules fabricated by common 4-inch wafer facilities. In the future, the driving voltage would be decreased and different functionalities would be implemented to realize lab-on-a-wristband (LOW) using the relative large area around patients' wrists for point-of-care (POC) applications.

[a]*Department of Material Science and Engineering, National Chiao Tung University, 207, Engineering 1, 1001 University Road, Hsinchu, Taiwan. E-mail: skfan@mail.nctu.edu.tw; Fax: +886-3-5729912; Tel: +886-3-5712121 ext. 55813*

[b]*Department of Mechanical Engineering, National Chiao Tung University, Hsinchu, Taiwan. E-mail: whsu@mail.nctu.edu.tw; Fax: +886-3-5720634; Tel: +886-3-5712121 ext. 55111*

† Electronic supplementary information (ESI) available: PET machining by a razor blade cutter (Fig. s1); DOW modules (Fig. s2); droplet actuation against gravity in inclined or curved devices (Fig. s3); speed of the droplet driven in the DOW (Fig. s4); video of droplet across a top plate gap (Video 1); video of droplet across a modular interface (Video 2); and video of droplet driven in the DOW (Video 3). See DOI: 10.1039/c0lc00178c

## Design and experiments

### Droplet transfer across top plate gap

Although electrowetting-based droplet manipulations have been demonstrated between parallel plates or on an open surface with patterned electrodes[21,22] for numerous applications,[23–25] transferring droplets was only demonstrated by manual soft printing from one device to a blank glass substrate.[26] Transferring a droplet across a gap would be a milestone to enrich the digital microfluidic functions after generating, transporting, merging, and splitting droplets have long been demonstrated.[18,19] Here the digital microfluidic modular interface was studied based on the parallel-plate electrowetting devices. Because the modular interface was designed to be easy-to-attach/detach, a gap between closely placed modules without sealing is desirable. To investigate the largest gap for a droplet to move across, we designed a device with two separate top plates as shown in Fig. 1(a). After several trials of using glass top plates, we found the kerfs (i.e., sidewalls and edges) of the top plates machined by a diamond scribe were not clean and smooth, which hindered the droplet transferring and even caused leakage from the top gap and dead volume leaving liquid in the gap. Therefore, we later employed PET (polyethylene terephthalate) as the substrate material because it is easily machined and cut to bring sharp and perpendicular sidewalls (see Fig. s1(a) in the ESI†) by our home-made razor blade cutter (see Fig. s1(b) in the ESI†). In addition to the machining purposes, PET is an ideal substrate material for microfluidic modules because flexible and compliant PET substrates are easily adjustable and aligned during module assembly.

After cutting PET substrates to appropriate dimensions, the following microfabrication processes, slightly different from those of a glass electrowetting device,[27,28] were performed. According to the thermal stability of our 175 μm-thick PET with ITO coating (indium tin oxide, 100 Ω/sq resistivity) provided by Join Well Technology, the resistivity increment should be less than 10% after 30 min heat treatment at 150 °C. To ensure no degradation of the PET and ITO, we conducted all the curing steps below 90 °C. Moreover, the chemical stability of PET was first tested by immersing the ITO PET substrates in the chemicals used in our microfabrication processes for 10 min. After testing, both ITO and PET were not attacked in isopropyl alcohol, acetone, FHD-5 (developer for positive photoresist), and PGMEA (propylene glycol monomethyl ether acetate, SU-8 developer).

The square driving electrodes ($W = 1.5$ mm in Fig. 1(b)) on the bottom plate were patterned by wet etching with BOE at room temperature using positive photoresist FH-6400 (Fujifilm Olin) as the etching mask. A 1 μm-thick SU-8 (MicroChem) layer was then spun, exposed, developed, and baked to be the dielectric layer above the electrodes. Finally, 66 nm-thick Teflon (DuPont) was coated to make the surface hydrophobic (water contact angle ~110°). The top plates were prepared by coating Teflon on ITO PET substrates. Before spinning Teflon, the edges of the top plates needed to be wetted by Teflon solution to ensure the hydrophobicity of the sidewalls for preventing leakage and dead volume mentioned above.

During experiments, the heights of the channel and the droplets ($d$ in Fig. 1(a)) were fixed to be 500 μm. To test the gap ($g$ in Fig. 1(a) and 1(b)) effect on different droplet volumes, 1.5, 2.5, and 3.5 μl droplets were driven across 50, 200, and 350 μm-wide gaps by grounding the two top reference electrodes (denoted by R and R′ in Fig. 1(a) and 1(b)) and sequentially energizing the bottom driving electrodes through a three-phase-bus.[29] Three subgrouped driving electrodes indicated by 1, 2, and 3 in Fig. 1 were electrically accessed through switches controlled by the LabVIEW software to build a droplet pathway.

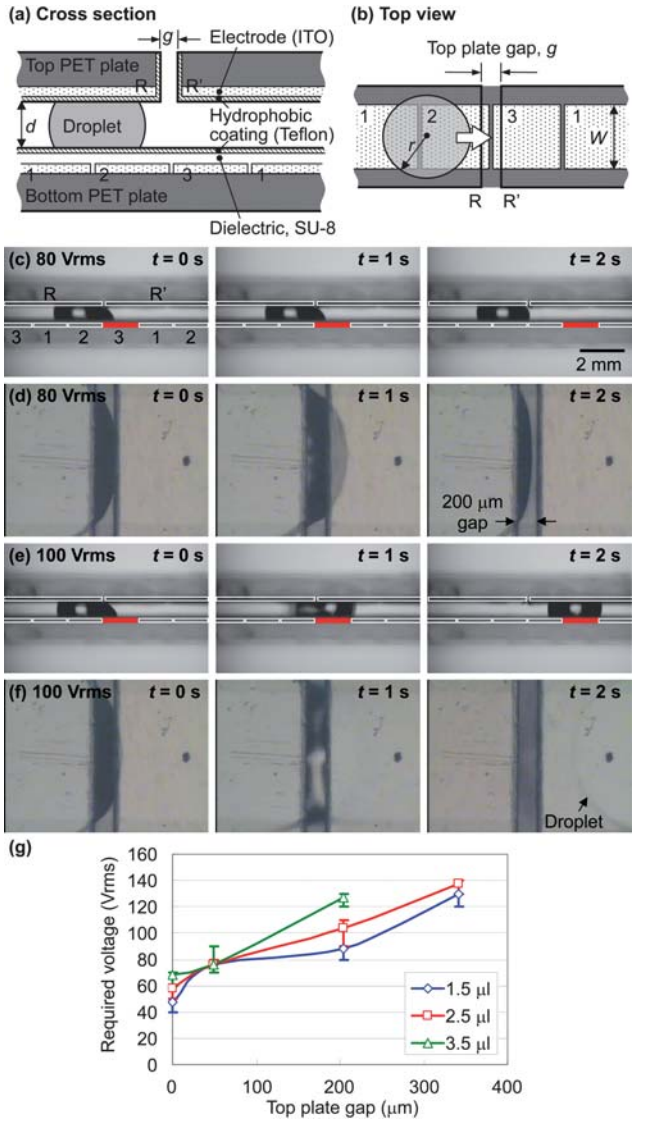


**Fig. 1** Transferring droplets across a top plate gap. (a) Cross section and (b) top view of the test device with two top plates separated by $g$. (c) Side view and (d) top view of a 2.5 μl DI water droplet failing to pass a 200 μm-wide gap when 80 Vrms and 2 kHz electric signal was applied on the 1.5 mm × 1.5 mm driving electrodes at the switching rate of 1 Hz. (e) Side view and (f) top view of a droplet pumped across the gap by applying 100 Vrms. The video of (e) can be seen in Video 1 in the ESI.† (g) The required voltage plotted against the top plate gap (0, 50, 200, and 350 μm) for droplet with different volumes of 1.5, 2.5, and 3.5 μl.

Fig. 1(c) and 1(d) show the side and top views, respectively, of a 2.5 μl deionized (DI) water droplet failing to pass across

 

a 200 μm-wide gap by applying an 80 Vrms and 2 kHz sine wave on each highlighted driving electrode for 1 s. As indicated in Fig. 1(c) and 1(d), the highlighted driving electrode 3 was turned on between $t = 0$ s and $t = 1$ s; driving electrode 1 was powered between $t = 1$ s and $t = 2$ s. Although the droplet was extended and extruded on the powered electrode 3 ($t = 1$ s), it was not successfully transferred from one top plate (R) to the other (R′). When the sine wave signal was switched from electrode 3 to electrode 1 ($t = 2$ s), the droplet did not follow the signal to move forward. As we increased the applied voltage to 100 Vrms, the droplet was able to touch electrode R′ ($t = 1$ s) and be pumped across the gap ($t = 2$ s) without leakage and dead volume as shown in Fig. 1(e) and (f). Video 1 in the ESI† demonstrates the droplet crossing the gap back and forth (Fig. 1(e)). From the recorded videos, jumping of the contour line of the droplet to touch the next top plate is crucial to successful droplet transferring but its mechanism is not fully understood. We speculate that the voltage application generated not only the pumping pressure but also some oscillation[30,31] of the droplet to touch the next top plate. A high speed camera would help to comprehend the sudden jumping and to improve the gap-crossing process in the future. The required minimum voltages to cross over different gaps, 0, 50, 200, and 350 μm, back and forth were measured and plotted in Fig. 1(c). In general, higher voltage was needed for a larger droplet passing across a larger gap. The maximum 140 Vrms used in the experiments was not sufficient to transport a 3.5 μl droplet across the 350 μm-wide gap. In real applications, 80 Vrms would be sufficient to transfer droplets because the two top plates can be placed as close as possible making the gap smaller than 50 μm.

### Modular interface for chip-to-chip droplet transportation

The modular interface is designed to transfer not only the droplets but also the electrowetting signals. Based on the top plate gap study, two closely neighbored modules with overlapping plates and complementary electrodes were designed as shown in Fig. 2. Similar to the previous study, the droplet was driven by grounding the reference electrode (R and R′) and sequentially applying voltage on the driving electrodes (1/1′, 2/2′, and 3/3′). The electrodes indicated with the same letter or number were electrically connected, while the prime (′) sign is used only to distinguish the two modules. The top plate of the left module partially overlapped the bottom plate of the right module with vertically matching electrodes including reference, driving, and interface electrodes. In addition to the matching pairs 2-R′, 3-3′, and R-1′ in the overlapping region (Fig. 2), four corresponding interface electrodes on each module were designed for electric connections (*i.e.*, connecting 1-1′, 2-2′, 3-3′, and R-R′) through appropriate spacers with conductive vias (vertical interconnect accesses) shown in the B–B′ cross section of Fig. 2(b).

Fig. 2(c)–(h) demonstrate a 2.5 μl droplet moving across two 50 μm-wide gaps of a modular interface. The height ($d$) of the spacer or the droplet was 500 μm, and the driving electrodes were 1.5 mm × 1.5 mm. By switching a sufficient electric signal (*i.e.*, 2 kHz and 80 Vrms sine wave) from electrodes 1/1′ (indicated by arrows in Fig. 2(d)) to 2/2′ (Fig. 2(e)), the droplet was pumped from the left module across the bottom gap to the overlapped region. Fig. 2(f) shows that the droplet was elongated

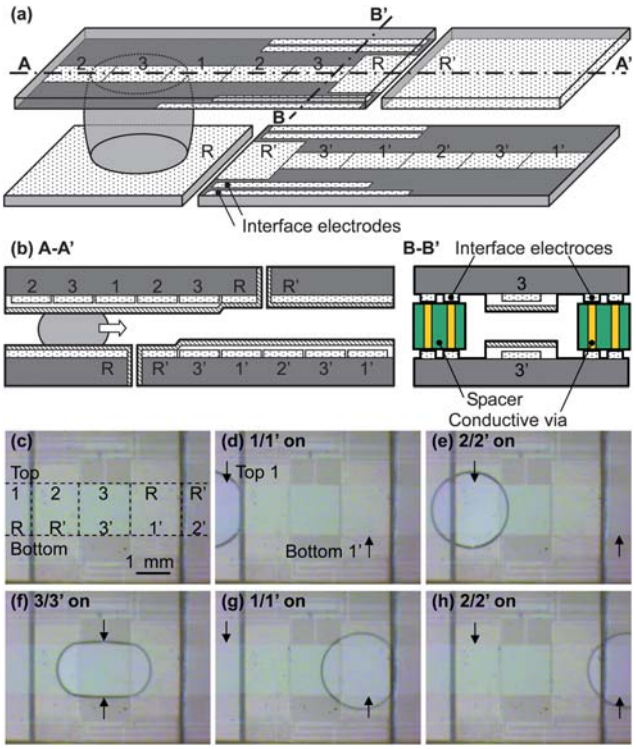


**Fig. 2** Modular interface design and test for chip-to-chip droplet transportation. (a) Sketch of the interface between two modules with an overlapping region and two gaps. (b) The AA′ and BB′ cross sections of (a). In the overlapping region, electrode pairs 2-R′, 3-3′, and R-1′ are vertically opposing to each other. The electric conections between 1-1′, 2-2′, 3-3′, and R-R′ are provided by the interface electrodes and conductive vias in the insulating spacer. (c) Top view of the modular interface indicating the electrodes. (d)–(h) Transferring a 2.5 μl droplet from the left module (d), across the left bottom gap (e), through the overlapping region (f)–(g), and across the right top gap (h) toward the right module by applying 80 Vrms and 2 kHz to the arrow-indicated electrodes at a switching rate of 1 Hz. (See Video 2 in the ESI.†)

and positioned at the center of the overlapped region, when the electrodes 3/3′ were powered. By sequentially switching the voltage among the three subgroups of the driving electrodes, the droplet was transferred from the overlapped region, across the top gap, and toward the right module as shown in Fig. 2(g) and (h). The switching rate was 1 Hz as can be seen in Video 2 in the ESI.†

### DOW with flexible modules

After understanding the gap effect and achieving droplet transportation across a modular interface, we further exploited the flexibility characteristic of PET and tried to demonstrate the DOW composed of four modules, shown as module I, II, III, and IV in Fig. 3(a). Module I and III were similar, except that module I included additional contact pads for the electric signals of the whole DOW as shown in Fig. 3(a). The inner plate of module I and III was a 7.5 mm-long and 15 mm-wide PET substrate containing a blank reference electrode. Nine driving electrodes, 2 reference electrodes and 8 interface electrodes were patterned on the outer plate of module III (16.8 mm-long and 15 mm-wide)

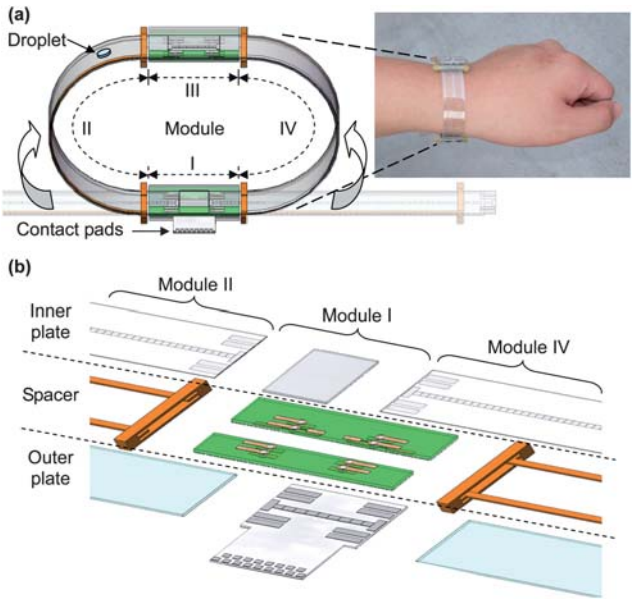


**Fig. 3** Droplet-on-a-wristband (DOW). (a) The sketch of the DOW composed of four flexible modules. The inset shows the DOW wearable on the wrist. (b) Explosion view of the module I and part of the module II and IV. Each module contains three layers: inner plate, spacer, and outer plate.

and on the major part of that of module I. Two spacers containing conductive vias for electric connections between the inner and outer plates and between the modules were placed in module I (Fig. 3(b)) and III. The assembled module I can be seen in Fig. s2(a) in the ESI.†

Module II and IV were identical, containing 59 driving electrodes, 2 reference electrodes, and 8 interface electrodes on each inner PET plate which was 92.7 mm-long and 15 mm-wide. Blank reference electrodes were deposited on the 86.3 mm-long and 15 mm-wide outer plates. A 500 μm-thick flexible PC (polycarbonate) spacer was placed between the inner and outer plates to provide a constant gap between the plates even when the module was bent. More detailed sketch of assembled module II and IV can be seen in Fig. s2(b) in the ESI.†

During assembly, module II and IV were first connected to module I using the described modular interface (Fig. 3(b)) and then bent and connected to module III (Fig. 3(a)). After assembly, glass plates were placed above and under module I and III for fastening the DOW with proper clamps. Finally, the DOW with a circumference of 204 mm (8 inch) was assembled from four flexible modules fabricated by 4-inch wafer facilities, yielding a large fluidic track that can be worn on the wrist as shown in the inset of Fig. 3(a). The radius of the curved module II and IV was around 25 mm (*i.e.*, curvature of 0.04 $mm^{-1}$).

Before transporting droplets in the DOW, we performed more fundamental experiments of droplet driving against gravity. Different from demonstrated droplet handlings on an open curved surface,[32] here we measured the minimum required voltage to drive a droplet by electrowetting between plates with specified inclined angles or curvatures. Similar to the above experiments, 2.5 μl DI water droplets were pumped in a 500 μm-high channel between plates by applying a 2 kHz electric signal to the 1.5 mm × 1.5 mm driving electrodes. The experimental setup and results of the inclined plate tests are shown in Fig. s3(a) and s3(b) in the ESI,† respectively. As the inclined angle increased from 0, 30, 60, to 90°, the required voltage to drive the droplet upwards along 45 successive driving electrodes at the switching rate of 1 Hz became larger to overcome the increased gravity force. Basically, the square of the required voltage (electrowetting force) would be proportional to the sum of the friction force mainly from contact angle hysteresis and the sine function of the inclined angle (gravity force), which can be seen in the experimental results. In the curved plate tests, jigs with different curvatures were fabricated and vertically positioned making the tangent to the curved jig at the center point vertical to the ground as shown in Fig. s3(c) in the ESI.† Droplets were pumped from the bottom, through the center point, and toward the top along the 45 driving electrodes of the tested device mounted on the curved jigs. The required voltage for different curvatures, 0, 0.02, 0.04, and 0.06 $mm^{-1}$, were measured and plotted in Fig. s3(d) in the ESI.† The tested curvatures were far less than the critical one causing damage of ITO or PET[33] but reasonable for wearable devices. Because the largest gravity that electrowetting needed to overcome occurred at the center point, the required driving voltages were not noticeably dependent on the different curvatures and similar to that required for 90°-inclined devices. In both the inclined and curved plate tests, 80 Vrms was sufficient in all the tested inclined angles and curvatures.

Based on the above studies, a 2.5 μl DI water droplet should be successfully driven in the assembled DOW with the 0.04 $mm^{-1}$ curvature and across the gap between modules. Fig. 4 shows the captured images of a video (Video 3 in the ESI†) recording the clockwise movement of a 2.5 μl droplet on the 204 mm-long droplet track in the DOW at a speed of 15 mm $s^{-1}$ by switching the applied voltage of 100 Vrms and 2 kHz at a rate of 10 Hz among a total of 136 driving electrodes. Droplet driving at higher

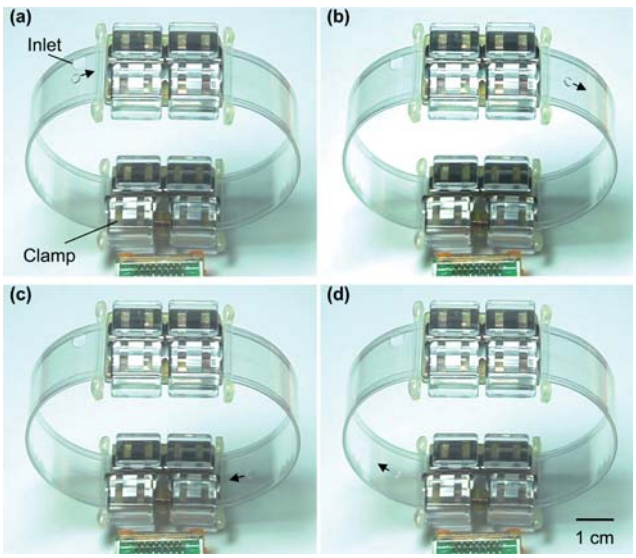


**Fig. 4** Continuous droplet transportation on the 204 mm-long droplet track in the assembled DOW with four flexible modules and four modular interfaces. Clamps and glass plates were used to fasten the DOW, making it easy-to-attach/detach. (a)–(d) A 2.5 μl droplet was pumped at a speed of 15 mm $s^{-1}$ by switching the applied 100 Vrms among the entire 136 driving electrodes. (See Video 3 in the ESI.†)

 

switching rates up to 70 Hz (*i.e.*, 105 mm $s^{-1}$) and in the counterclockwise direction was investigated as shown in Video 3 and Fig. s4 in the ESI.†

## Conclusion

Based on the studies of droplet transportation across a top plate gap, through a modular interface, between inclined and curved plates, we implemented modular digital microfluidic LOC with easy-to-attach/detach modules. The presented modular interface for chip-to-chip droplet transportations can be applied to channel-based continuously microfluidic modules with proper digital-to-channel interfaces.[20] A 2.5 μl droplet was transported against gravity on an 8 inch-long track in the DOW assembled by four flexible modules fabricated by less expensive 4-inch wafer facilities. By replacing the currently used 1 μm-thick SU-8 with a thinner dielectric thin film with a higher dielectric constant, the driving voltage would be decreased for safely wearing the DOW on the wrist. The large area of each replaceable module can be further functionalized for specific LOW applications in the future.

## Acknowledgements

The authors would like to thank the Nano Facility Center at National Chiao Tung University, Hsinchu, Taiwan for providing fabrication facilities, and the Join Well Co., Ltd for supporting the ITO PET films and related technical services. This work is partially supported by the National Science Council, Taiwan, under grants NSC 95-2218-E-009-023 and NSC 98-2221-E-009-129-MY3.

## Reference

1 G. M. Whitesides, *Nature*, 2006, **442**, 368–373.
2 T. M. Squires and S. R. Quake, *Rev. Mod. Phys.*, 2005, **77**, 977–1026.
3 N.-T. Nguyen and Z. Wu, *J. Micromech. Microeng.*, 2005, **15**, R1–R16.
4 T. Nguyen, J. P. Hilton and Q. Lin, *Microfluid. Nanofluid.*, 2009, DOI: 10.1007/s10404-008-0400-7.
5 Y. Kang and D. Li, *Microfluid. Nanofluid.*, 2009, DOI: 10.1007/s10404-009-0408-7.
6 D. Mark, S. Haeberle, G. Roth, F. von Stetten and R. Zengerle, *Chem. Soc. Rev.*, 2010, **39**, 1153–1182.
7 U. M. Attia and J. R. Alcock, *Int. J. Adv. Manuf. Technol.*, 2009, DOI: 10.1007/s00170-009-2345-8.
8 D. Erickson and D. Li, *Anal. Chim. Acta*, 2004, **507**, 11–26.
9 J. Melin and S. R. Quake, *Annu. Rev. Biophys. Biomol. Struct.*, 2007, **36**, 213–231.
10 T. Thorsen, S. J. Maerkl and S. R. Quake, *Science*, 2002, **298**, 580–584.
11 K. Sun, Z. Wang and X. Jiang, *Lab Chip*, 2008, **8**, 1536–1543.
12 P. Grodzinski, J. Yang, R. H. Liu and M. D. Ward, *Biomed. Microdevices*, 2003, **5**, 303–310.
13 K. A. Shaikh, K. S. Ryu, E. D. Goluch, J.-M. Nam, J. Liu, C. S. Thaxton, T. N. Chiesl, A. E. Barron, Y. Lu, A. Mirkin and C. Liu, *Proc. Natl. Acad. Sci. USA*, 2005, **102**, 9745–9750.
14 P. K. Yuen, *Lab Chip*, 2008, **8**, 1374–1378.
15 S. Miserendino and Y.-C. Tai, *Sens. Actuator A-Phys.*, 2008, **143**, 7–13.
16 C. K. Fredrickson and Z. H. Fan, *Lab Chip*, 2004, **4**, 526–533.
17 J. Atencia, G. A. Cooksey, A. Jahn, J. M. Sook, W. N. Vreeland and L. E. Locascio, *Lab Chip*, 2010, **10**, 246–249.
18 M. G. Pollack, R. B. Fair and A. D. Shenderov, *Appl. Phys. Lett.*, 2000, **77**, 1725–1726.
19 S. K. Cho, H. Moon and C.-J. Kim, *J. Microelectromech. Syst.*, 2003, **12**, 70–80.
20 M. Abdelgawad, M. W. L. Watson and A. R. Wheeler, *Lab Chip*, 2009, **9**, 1046–1051.
21 R. B. Fair, *Microfluid. Nanofluid.*, 2007, **3**, 245–281.
22 U.-C. Yi and C.-J. Kim, *J. Micromech. Microeng.*, 2006, **16**, 2053–2059.
23 M. Abdelgawad and A. R. Wheeler, *Adv. Mater.*, 2009, **21**, 920–925.
24 N. A. Mousa, M. J. Jebrail, H. Yang, M. Abdelgawad, P. Metalnikov, J. Chen, A. R. Wheeler and R. F. Casper, *Science Translational Medicine*, 2009, **1**, 1–6.
25 R. Sista, Z. Hua, P. Thwar, A. Sudarsan, V. Srinivasan, A. Eckhardt, M. Pollack and V. Pamula, *Lab Chip*, 2008, **8**, 2091–2104.
26 U.-C. Yi and C.-J. Kim, *Sens. Actuator A-Phys.*, 2004, **114**, 347–354.
27 S.-K. Fan, H. Yang, T.-T. Wang and W. Hsu, *Lab Chip*, 2007, **7**, 1330–1335.
28 S.-K. Fan, P.-W. Huang, T.-T. Wang and Y.-H. Peng, *Lab Chip*, 2008, **8**, 1325–1331.
29 V. Srinivasan, V. K. Pamula and R. B. Fair, *Lab Chip*, 2004, **4**, 310–315.
30 J. M. Oh, S. H. Ko and K. H. Kang, *Langmuir*, 2008, **24**, 8379–8386.
31 F. Mugele, J.-C. Baret and D. Steinhauser, *Appl. Phys. Lett.*, 2006, **88**, 204106.
32 M. Abdelgawad, S. L. S. Freie, H. Yang and A. R. Wheeler, *Lab Chip*, 2008, **8**, 672–677.
33 B. M. Henry, A. G. Erlat, A. McGuigan, C. R. M. Grovenor, G. A. D. Briggs, Y. Tsukahara, T. Miyamoto, N. Noguchi and T. Niijima, *Thin Solid Films*, 2001, **382**, 194–201.